Ray Tracing Simulation Techniques for Understanding High Resolution SAR Images

Stefan Auer, *Member, IEEE*, Stefan Hinz, *Member, IEEE* and Richard Bamler, *Fellow, IEEE*

Abstract

In this paper a simulation concept is presented for creating SAR reflectivity maps based on ray tracing. Three-dimensional models of man-made objects are illuminated by a virtual SAR sensor whose signal is approximated by rays sent through the model space. To this end, open source software tools are adapted and extended to derive output data in SAR geometry followed by creating the reflectivity map. Rays can be followed for multiple reflection within the object scene. Signals having different multiple reflection levels are stored in separate image layers.

For evaluating potentials and limits of the simulation approach, simulated reflectivity maps and distribution maps are compared with real TerraSAR-X images for various complex man-made objects like a skyscraper in Tokio, the Wynn Hotel in Las Vegas and the Eiffel Tower in Paris. The results show that the simulation can provide very valuable information to interpret complex SAR images or to predict the reflectivity of planned SAR image acquisitions.

Re-print of:
Auer, S.; Hinz, S.; Bamler, R., "Ray Tracing Simulation Techniques for Understanding High Resolution SAR Images", IEEE Transactions on Geoscience and Remote Sensing, vol. 48, no. 3, pp. 1445-1456, March 2010

Index Terms

SAR simulation, Ray Tracing, POV Ray, Radar Scattering, 3D Modelling, TerraSAR-X

I. Introduction

After high resolution radar satellite missions like TerraSAR-X or Cosmo-Skymed have been launched in 2007, spaceborne SAR images reach spatial resolutions below one meter in azimuth and range in spotlight mode [1] [2]. Due to the increased resolution, only few scatterers are located within one resolution cell. Hence, new deterministic

Manuscript received Month, Day, Year: revised Month, Day, Year.

S. Auer is with Remote Sensing Technology, Technische Universität München (TUM), Germany, e-mail: Stefan.Auer@bv.tum.de

S. Hinz is with the Institute of Photogrammetry and Remote Sensing, Universität Karlsruhe (TH), Germany, e-mail: stefan.hinz@ipf.uni-karlsruhe.de

R. Bamler is with the Remote Sensing Technology Institute (IMF), German Aerospace Center (DLR), Oberpfaffenhofen, Germany, and with Remote Sensing Technology, Technische Universität München (TUM), Germany, e-mail: Richard.Bamler@dlr.de

components occur especially at man-made objects causing bright image features [3] [4], what is most apparent for strong backscattering at building walls. Texture information within the image has become more meaningful what supports the interpretation of SAR images. Furthermore, the number of strong scatterers is increased drastically within urban areas and extended linear or areal structures now show long-term stable scattering behavior, which can be seen as a paradigm change in persistent scatterer interferometry [5] [6] [7].

Although more details are distinguishable in high resolution SAR images, visual analysis of the geometrical distribution of features still turns out to be challenging and time consuming. Figure 1, showing the ”Maison de Radio France” in the center of Paris, gives an example for reflection effects appearing in urban areas which are difficult to explain: while the geometrical structure is obvious in the optical image (left), interpretation of reflection effects in the SAR mean amplitude map, which has been created by averaging six spotlight TerraSAR-X images, is not straightforward. Hence, creating artificial SAR images or reflectivity maps by means of simulation methods has proven to be helpful for supporting the interpretation of reflection effects in the azimuth-range plane.

In the published literature, basically two groups of approaches can be found. Approaches focusing on *radiometric* correctness use formulas in closed form for providing intensity values of high quality comparable to real SAR images while the level of detail of 3D models to be used is limited. E.g. Franceschetti et al. developed SARAS [8] and added reflection models for describing multiple bounce effects at buildings approximated by box models [9] [10]. The second group of simulation approaches concentrates more on the *geometrical* correctness of the simulation.

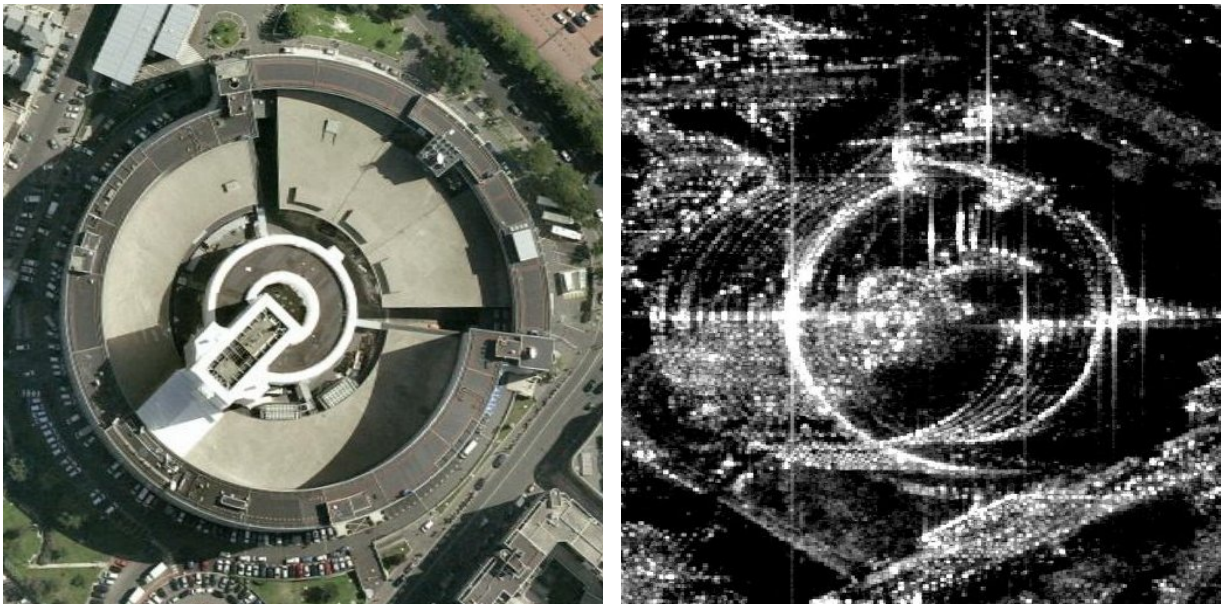

(a) Birds eye view; ©Google Earth (b) SAR mean map

Fig. 1: Maison de Radio France (Paris): obvious geometry in optical image; challenging interpretation in TerraSAR-X mean map (spotlight mode, azimuth direction bottom-up; range direction from left to right)

Balz [11] used programmable graphics card units for generating single bounce SAR images in real time. Margarit et al. analyzed reflection effects, multiple reflection and SAR polarimetry by illuminating detailed 3D models of vessels [12] and buildings [13], while preserving high radiometric quality by using a radar cross section simulator [14]. Brunner et al. [15] show how to extract features from real SAR images by comparing them to simulated images. Hammer et al. [16] compared different simulation concepts for obtaining artificial SAR images.

Our simulator also uses ray tracing tools. However, in contrast to the other approaches, the core tracing algorithms are taken from the open-source software package "POV Ray" which was originally developed for simulating optical images. This allows us to concentrate on modelling the specific SAR scattering effects, e.g. tracing rays through multiple reflecting and storing signals of different bounce levels in separated image layers. Effects caused along the synthetic aperture and during SAR focusing are approximated by using a cylindrical light source and an orthographic camera for modeling the SAR antenna.

The motivation and novelties of this approach are outlined in Section II followed by a detailed explanation of the simulation process in Section III. Afterwards, results of simulation are compared and assessed with real TerraSAR-X images in Section IV. Finally, potentials and limitations of the simulator are concluded and future work to be done is summarized in Section V.

II. Motivation

The aim of this work is to develop a software tool offering the possibility for simulating backscattering effects showing up in high resolution SAR images. Furthermore, reflection contributions of different bounce levels are to be displayed in separated image layers. Since deterministic scattering effects mostly appear at man-made objects, multi-body urban scenes are of special interest. Simulated reflectivity maps can be used for supporting the interpretation of real SAR images, for predicting backscattering effects in SAR images and for detecting and grouping strong point scatterers [17] which are used, for instance, in Persistent Scatterer Interferometry [18] [19].

Guida et al. [20] use closed equations to analyze deterministic backscattering effects appearing in high resolution TerraSAR-X images. Hence, some restrictions have to be accepted at the cost of high radiometric quality: simulation results using meshed LIDAR data are limited to single scattering and 3D-models of buildings are designed by parallelepipeds without roof structures. In our approach, for being able to analyze multiple scattering in more complex three-dimensional model scenes, we put more focus on the geometrical correctness of the distribution of scattering effects. Radiometric proportions between different bounce levels as well as speckle noise are of less importance and are only approximated.

In particular the following requirements should be fulfilled:

- the complexity of 3D models to be included should be high in order to be able to detect reflection phenomena appearing at small building features
- separation of different bounce levels should be feasible by counting the number of reflections for each ray followed through the modeled scene

- rays should be followed through the entire modelled scene to enable geometrical analysis like location of intersection points, analyis of reflection angles, etc.
- both reflection models, specular and diffuse, as well as parameters for controlling the reflectivity of surfaces should be available

These requirements led us to the conclusion to base the developments on an existent software tool: POV Ray (Persistence of Vision Ray, [21], [22] [23]), a well known ray tracer for generating virtual optical images, and modify it in such a way, that it can deliver output data for generating images in SAR geometry.

In our opinion, POV Ray fitted well into the defined requirement profile since:

- it comprises a huge variety of very fast simulation tools
- basic modules are thoroughly tested and free from programming errors
- including own developments is possible due to free access to its source code
- the source code has been continuously developed and improved by a huge community since 1991
- it uses an efficient concept for tracing rays, more specifically: backwards ray tracing, which starts at the center of each image pixel and follows the ray backwards on its way to the light source

In the following section, the simulation concept is explained in more detail. Starting with the geometrical and radiometric description of objects, the process chain is continued by sampling the three-dimensional model scene by means of rays and is completed by the image creation for obtaining the reflectivity map in the azimuth-range plane.

III. Simulation Process

The simulation process consists of three major parts:

1) Scene modelling: in a first step, a 3D scene model has to be constructed and imported into the ray tracer
2) Sampling of model scene: by applying the ray tracing algorithm provided by POV Ray, the analysis for backscattering contributions is performed by tracing rays through the modelled scene. For defining both the origin and the direction of the rays, a virtual orthographic ”camera” is used, whose optical axis is aligned with the intended viewing direction of the radar sensor. While creating the synthetic image of the scene, coordinates in azimuth and slant range, intensity values and bounce levels are derived as output data for all intersection points detected at objects in the scene.
3) Creation of reflectivity map: the artificial reflectivity map is generated by assigning all intensity contributions - according to their azimuth and slant range coordinates - to elements of a regular grid in radar coordinates imposed onto the irregularly distributed data points derived during the prior sampling step.

A. Scene Modelling

A model scene to be used by a ray tracer has to contain the following elements: 3D scene objects to be illuminated, surface properties like reflectivity factors or the strength of diffuse/specular reflection for each object face, a camera

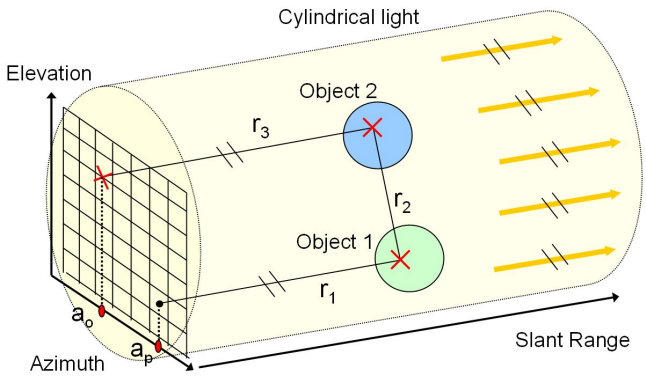

Fig. 2: Simulation concept: scene imaged by orthographic camera while two objects are illuminated by a cylindrical light source; a_o, a_p: coordinates to be used for calculation of phase center in azimuth; r_1, r_2, r_3: depth values for determination of slant range coordinate; slant range coordinate of double bounce contribution determined by $(r_1 + r_2 + r_3)/2$

at the position of the observer and at least one light source. The quality of images derived by ray tracing methods depends in particular on the quality of the modeled scene. While simple surfaces and standard objects like triangles, spheres, boxes, cylinders, etc. are easily created, complex objects can be formed by means of Constructive Solid Geometry (CSG) [24] including set-operations like 'union', 'difference' or 'intersection' for composing complex objects from simple primitives. Moreover, besides some other formats which still have to be tested, the following 3D model formats have been successfully imported into POV Ray: Object format (.obj), 3DS max (.3ds) and SketchUp (.skp).

To generate a synthetic backscatter image of the scene, the virtual sensor is modeled by means of two components: i) a cylindrical light source emitting parallel light rays for simulating the azimuth focused SAR signal and ii) an orthographic sensor, for modelling the receiver antenna, both at the same position and with coinciding viewing direction. Using an orthographic sensor offers the possibility to determine the phase center position of each scattering contribution in azimuth and range direction. As the simulator scans the modeled scene by means of rays, the density of the sampling process depends on the geometrical resolution of the sensor, i.e. the synthetic image.

Considering the radiometric model for the simulation, we rely on standard models, since our focus is on geometrical quality of the result. Intensity values are evaluated at object surfaces by means of a combination of a diffuse and a specular reflection model.

For estimating the diffuse intensity contribution I_d, the following equation is applied:

$$I_d = k \cdot I \cdot \left(\overrightarrow{N} \cdot \overrightarrow{L}\right)^b \tag{1}$$

where k is a diffuse reflection factor and I the intensity of the incoming signal. Lambertian reflectance is considered by the scalar product of the normalized vector $\overrightarrow{L}$ pointing in direction to the light source and the

normalized surface normal $\overrightarrow{N}$, which is 1 in the case of $\overrightarrow{L} = \overrightarrow{N}$. Parameter b can be adapted for approximating the backscattering behavior of metallic surfaces.

The reflection model for evaluating the specular reflected intensity I_s is defined as follows:

$$I_s = s \cdot \left(\overrightarrow{N} \cdot \overrightarrow{H}\right)^{\frac{1}{r}} \tag{2}$$

where s represents the reflectivity coefficient of the surface and r a roughness factor defining the sharpness of specular highlights. Normalized Vector $\overrightarrow{H}$ is the bisection vector [25] between the vector $\overrightarrow{L}$ pointing in direction to the light source and the direction vector $\overrightarrow{V}$ of the reflected ray whose intensity contributions have to be estimated. Eventually, diffuse and specular intensities are summed up for each signal reflection detected within the 3D model scene.

Both the specular and the diffuse reflection model have been originally developed for optical light [26] [27]. Hence, for improving the radiometric quality of the result in the future, both reflection models could be replaced by more appropriate models adapted to the wavelength of SAR signals, e.g. the Kirchhoff Approach (KA) or the Small Perturbation Method (SPM) [28]. However, replacing reflection models currently used for simulation would yet heavily increase the computing time of the simulator.

B. Sampling of Model Scene

A SAR imaging system maps the 3D world into a cylindrical co-ordinate system. It employs central perspective in the elevation direction and orthographic scanning in azimuth. For spatially limited areas, e.g. individual buildings, and space-borne geometry the central perspective in elevation can be well approximated by orthographic projection. This has several advantages: First, a 2D orthographic camera type is readily available in POV Ray and Second, having a constant incidence angle offers the possibility of zooming into the 3D model scene in order to analyze signal backscattering from features of interest like roofs, balconies or facades. The modelling of shadow is solved by including a cylindrical light source emitting parallel light. Thereby, a shadow test can be performed along all scan positions in azimuth. Moreover, equal signal intensities are guaranteed for all objects illuminated in the local area of interest.

The intensity contributions of the synthetic image are acquired by backwards ray tracing [25] and shall be explained in case of the model scene shown in Figure 2. The term ”backwards” refers to the fact that tracing starts at the receiving sensor and continues until the light source is reached or is aborted due to geometrical or radiometric constraints. Starting at the center of each image pixel, one ray, commonly called ’primary ray’, is constructed. Since the camera type is ’orthographic’, the direction of the ray is perpendicular to the image plane of the camera. Simultaneously, two default values are necessary for capturing characteristics of the reflection process to be analyzed. Firstly, the reflection level - which is referred to as ”bounce level” in the following parts of the paper - for counting the number of bounces along the ray’s path is set to 1. Moreover, in order to scale all intensity contributions derived throughout the modeled scene, a weight factor is introduced for the ray having a weight of 1.

The search for contributions is started at the center of each image pixel by following the ray along its path and seeking for intersections with the modeled scene. If the ray hits more than one object the intersected surface having the smallest spatial distance to the pixel center is treated as 'visible' and checked for color contributions, i.e. the intensity backscattered at the surface of object 1 is evaluated by calculating the specular and diffuse reflection component caused by the illumination of the light source, i.e. the virtual azimuth-focused SAR signal.

Afterwards, using both the intersection point and the surface normal at object 1, a secondary ray is created in specular direction and the bounce level is increased to 2. In this context, all rays constructed for trace levels higher than 1 are referred to as 'secondary rays'. The weight factor of the ray decreases according to the reflectivity factor of the surface of object 1, i.e. all further intensity contributions will be scaled by a value smaller than 1.

Tracing rays for the current pixel ends if the ray to be followed does not hit any further object, the maximum bounce level is reached or if the weight factor of the ray falls below a defined threshold. Both limits, bounce level and weight threshold, can be chosen by the operator. Eventually, all contributions are summed up for determining the intensity hitting the image pixel.

Concerning the calculating time, the duration of the simulation process highly depends on the number of pixels of the orthographic camera chosen for sampling the object scene, e.g. doubling the number of n pixels on each axis of the image plane requires the analysis of $4 * n$ rays, which all can finally reach a bounce level of 5. Influence of the complexity of imported 3D models on the processing time was remarkable but turned out to be much weaker than the influence of the image size.

C. Coordinates in Range and Azimuth

For computing slant range coordinates we have extended POV Ray's source code for extracting necessary depth information from the ray tracing process. In case of single bounce, the slant range distance R_s is directly given by the depth value of the first intersection point, i.e.

$$R_s = r_1 \tag{3}$$

If a double bounce appears, the slant range coordinate is derived by tracing the ray throughout the scene, until it hits the second face - in our example at object 2. Then, an additional ray has to be constructed, which is parallel to the primary ray and fixed at second intersection point. By intersecting this ray with the image plane of the orthographic camera, the origin of the ray at the virtual antenna is determined. Finally, according to Figure 2, the slant range coordinate R_d for double bounce is evaluated by half the sum over all three rays:

$$R_d = (r_1 + r_2 + r_3)/2 \tag{4}$$

For multiple bounces the procedure is easily extended since only the number of rays between objects and corresponding intersection points increases.

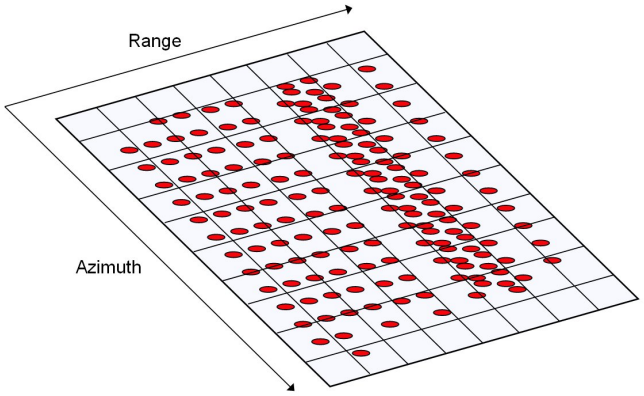

Fig. 3: Image creation: regular grid is imposed on detected reflection contributions (red points) followed by interpolation within each resolution cell

Triangular trihedral corner reflectors appear as a point in SAR images, even if the physical size of the reflector is larger than the spatial resolution of the SAR system [29]. This effect is accomodated in the simulator by averaging the azimuth coordinates A_o of the ray's origin at the antenna and the azimuth coordinate of the pixel center A_p where the primary ray was constructed (see Figure 2), i.e.

$$A = (a_p + a_o)/2 \tag{5}$$

Compared to the real SAR system, our simulator does not have to deal with ambiguities in azimuth and range. Both range and azimuth coordinates are obtained conserving best resolution.

Finally, as output data, the simulator stores one azimuth coordinate, one slant range coordinate, one intensity value and the bounce level for reflection effect detected along the path travelled by a ray.

Potential enhancements for the 3D analysis of reflection effects [30] [31] [32] will have to be investigated in the future by including the elevation direction as third dimension (Figure 2).

D. Creation of reflectivity map

The preceding steps showed how to derive necessary output data by means of our simulator. At this point, all intensity contributions are irregularly distributed in the azimuth-range plane since scanning of the scene in the SAR geometry yields areas with high point densities (caused by small angles between ray and object surfaces), lower point densities (caused by increased angles between ray and object surface) and also shadowed areas without any contributions. Hence, for obtaining the reflectivity map, a regular grid has to be imposed onto the illuminated area (see Figure 3). For each bounce level appearing in the scene one empty image layer is created, whose resolution in azimuth and range is chosen by the operator. As for the range direction, the operator can decide in favor of slant range or ground range what requires the specification of the radar incidence angle. After starting a loop over all

(a) Google Earth Model

(b) Birds eye view: pipe structures on one side of the roof

Fig. 4: Google Earth data; 3D model: level of detail: moderate, ©ynakamura, Google 3D gallery; optical image: ©Google Earth

contributions the sub-pixel coordinates are calculated for each intensity contribution whose intensity is added to the appropriate image layer by using the available bounce level information. For each bounce level requested by the operator, separate reflectivity maps are prepared and displayed. Moreover, since imposing a regular grid over an irregular point cloud may cause aliasing effects, the possibility of smoothing image layers by means of a bilinear filter has been included.

IV. Applications

In the following section, as all modeling and processing steps have been explained now, potentials and limitations of the simulator are shown by comparing simulated reflectivy maps with TerraSAR-X images. To this end, three locations with different kinds of complex objects have been chosen:

- a skyscraper in Tokio for detecting deterministic double bounce effects
- the Wynn Hotel in Las Vegas as an example for supporting detailed interpretation of multiple bounce effects
- the Eiffel Tower in Paris for detailed SAR simulation

In each case an available 3D model has been imported and sampled in POV Ray followed by creating the reflectivity map.

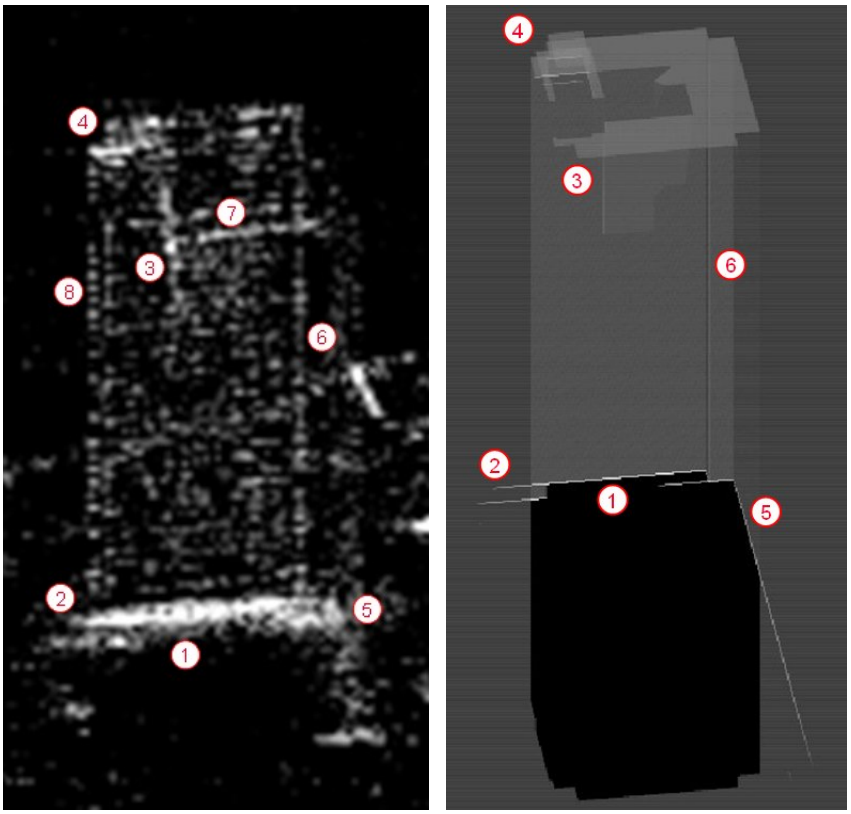

(a) TerraSAR-X image (b) Reflectivity map

Fig. 5: TerraSAR-X image (a) vs. Simulation (b); points 1 - 6: corresponding features; feature 7 not obtained by simulation; azimuth direction: left to right; slant range direction: top-down

A. Skyscraper

High resolution SAR sensors like TerraSAR-X or Cosmo Skymed provide images having a geometrical resolution of about one meter. Compared to the ENVISAT or ERS SAR data, fewer scatterers are located within one resolution cell causing less random interference between scattering contributions. Hence, more deterministic reflection effects become visible, especially in urban areas containing many man-made objects. In the following, this is exemplified for a TerraSAR-X image showing a skyscraper in Tokyo (Japan).

Within the Chuo-ku district of Tokyo, several skyscrapers are located next to the Aioi-bashi Bridge crossing the Sumida River. For one of these, the distribution of scattering effects has been analyzed by means of a Google Earth 3D model processed by our simulator. Both rotation angle of the building and incidence angle of the signal have been roughly estimated from the TerraSAR-X data and reflection properties have been assigned to all surfaces. Figure 4a shows a perspective view onto the building as seen by a spectator located at the position of the SAR sensor. In order to model double bounce effects caused by the surrounding ground, a flat plane with low diffuse

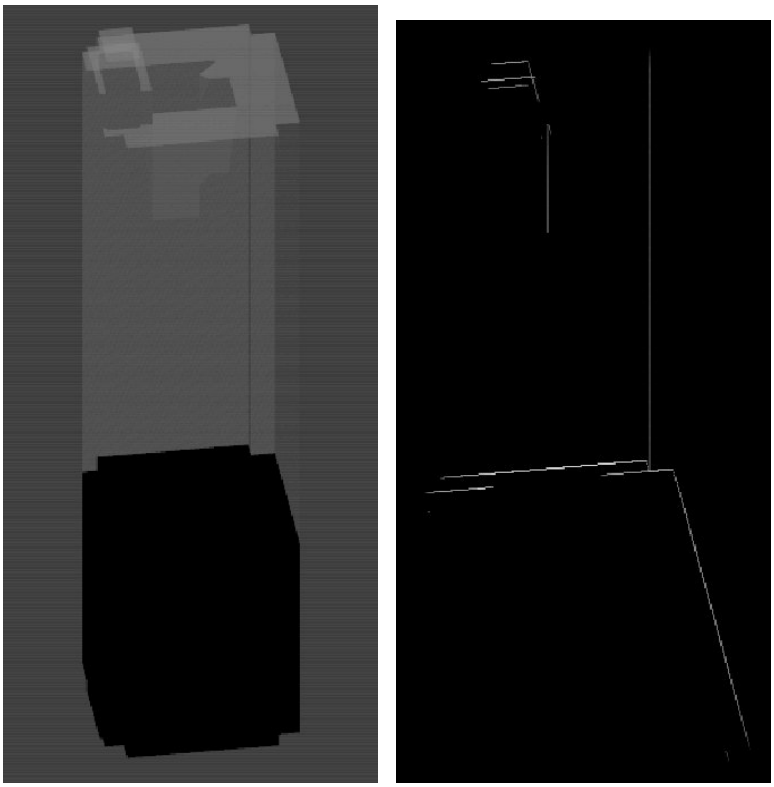

(a) Single Bounce (b) Double Bounce

Fig. 6: Separated layers for different bounce levels; azimuth direction: left to right; slant range direction: top-down

scattering characteristics has been introduced into the model scene. Since single bounce contributions show weak appearance at walls, the façades are modeled by closed surfaces showing strong specular reflection and low diffuse reflection.

Although the level of detail of the skyscraper model is only moderate, several similarities are clearly visible in the SAR image (Figure 5a) and the simulation result (Figure 5b). All double bounce contributions caused on the roof (feature 4), at wall corners, orientated in direction to the sensor, either on the inside of the building (feature 3) or on the outside of the building (feature 6), or by the interaction of walls and the surrounding ground (features 2 and 5) appear as linear structures and are much stronger than single bounce contributions. Lines of this kind appearing at the building's headwall are of special interest since their length depends 1.) on the building height and 2.) on the rotation angle of the building with respect to the line of sight of the sensor. Signals hitting higher regions of the rotated skyscraper's wall are reflected farther into the background of the building increasing the distance covered by the SAR signal back to the sensor. Consequences arising due to double bounce lines reaching beyond the ends of building walls should be taken into accound in the case of feature extraction in high resolution SAR images, even if this effect shows little occurrence for low buildings. For instance, Thiele et al. [33], whose

approach for building reconstruction in SAR images is based on the analysis of double bounce lines, report of a slight overestimation of building footprints extracted from multi-aspect high resolution SAR images.

In contrast to its long appearance in the reflectivity map, the double bounce line in the right part of the SAR image (feature 5) is much shorter since it is cut off by an adjacent building which has not been included in the POV Ray model scene (Figure 4a). Reflection contributions caused at roof features (feature 4) are clearly visible in both images while the gap in one of the horizontal double bounce lines (feature 1) is only hinted in the real SAR case. Compared to the SAR image, linear feature 7 (Figure 5a) does not show up in the simulation result. This reflection contribution is likely to be caused by a strong reflection effect at a step on the roof or by nearby metallic pipe structures which are shown in Figure 4b. A closer look at the skyscraper model in Figure 4a reveals that the step as well as the metallic pipes are not modelled in 3D since they have only been mapped as 2D textures on the flat roof surface.

Moreover, a vertical line of points (feature 8) is visible in the SAR image at the left end of the building which might appear due to backscattering at building edges or due to trihedrals at the façade of the building. For instance, Soergel et al. [34] analyzed edge scattering effects at urban buildings in the case of high-resolution air-borne SAR images. Contributions of trihedrals at the skyscraper's wall facing the SAR sensor can be clearly distinguished as focused points in the SAR image. However, these effects are missing in the reflectivity map since all building walls have been modeled by flat surfaces.

In addition to the reflectivity map, different bounce levels are displayed in separated layers for supporting the interpretation in more detail (see Figure 6). Concerning the comparability of intensities, the radiometric quality of the result is as limited as it was expected in advance. Even if the available reflection parameters had been optimized for all surfaces, radiometric errors would have appeared because of the discrete sampling of the 3D model scene, simplified reflection models for evaluating the backscattered intensity contributions and the separated treatment of each bounce along the ray's path.

B. Wynn Hotel

The second simulated reflectivity map uses a 3D model of the Wynn Hotel located in the center of Las Vegas, USA. By means of this example, it shall be shown that also 3D models of low quality can be used for supporting image interpretation, even if the SAR geometry is coarsely approximated.

A perspective view onto the curved building, which has been captured in Google Earth, is shown in Figure 7 and approximately indicates the line of sight of the sensor with respect to the hotel complex. A small lake called "Lake of Dreams" is visible in front of the hotel with a surface area of approximately 12.000 square meters. At one end of the lake an artificial waterfall is installed at a concave wall whose curvature is oriented in direction to the hotel (left part of Figure 8). This is done because, at the beginning of the afternoon, both lake and waterfall are illuminated for showing spectacular image sequences and color effects. The wall is curved, so that the same visual quality can be provided to all guests watching the show through the window of their hotel rooms.

By coincidence, the concave surface of the building is orientated perpendicular to the flight path of TerraSAR-X.

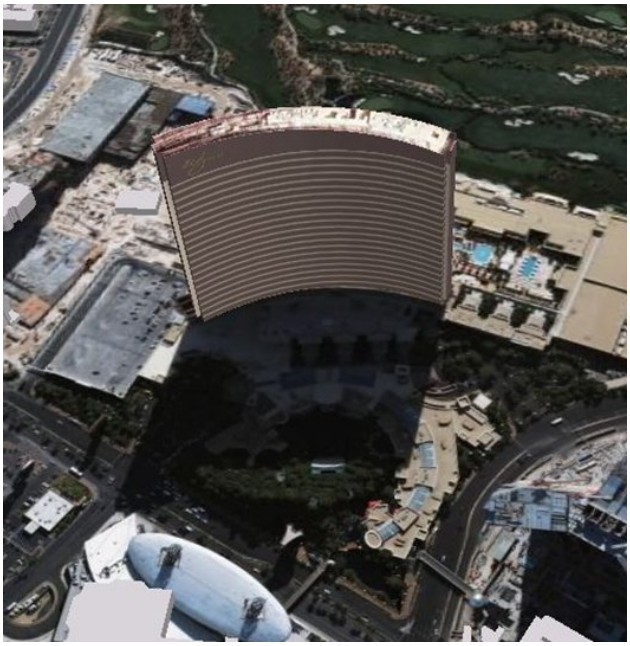

Fig. 7: Perspective view onto Wynn Hotel, Las Vegas (US); ”Lake of Dreams” situated in front of the building; ©Google Earth

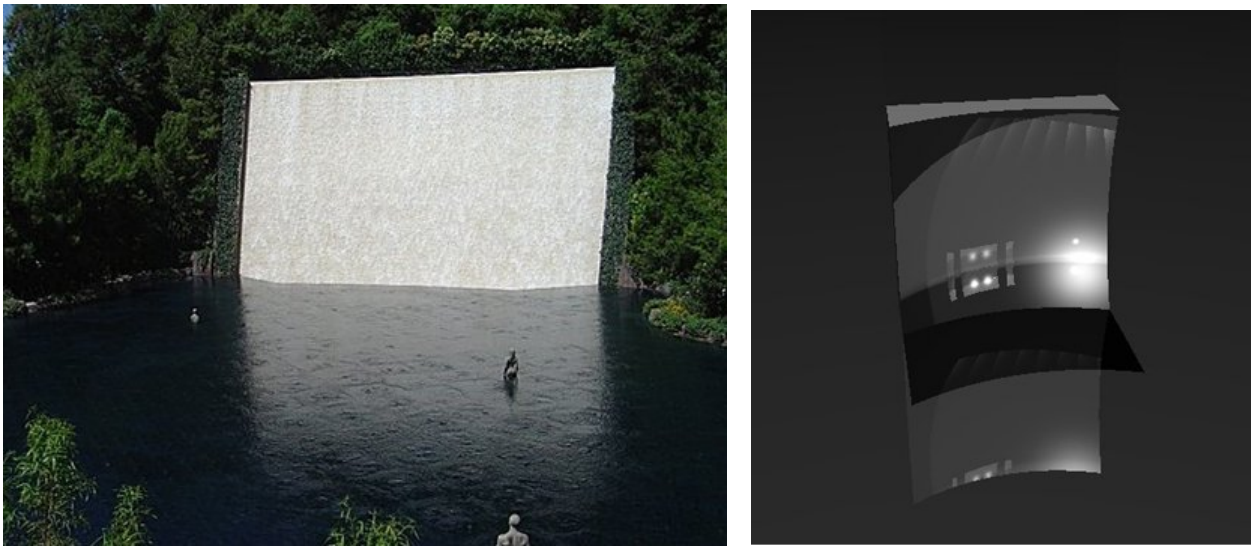

Fig. 8: ”Lake of Dreams”: water surface in front of waterfall (left), Google Panoramio, ©Pete & Sarah; concave model used for simulation derived by substracting a sphere from a cube (right)

In Figure 9, a spotlight image containing the hotel area is shown with range direction pointing top down. Firstly, strong reflection effects orientated in azimuth direction shall be considered from near to far range. The first eye catching feature looks like a curved rectangle whose transparent area seems to be framed by a bright border (feature

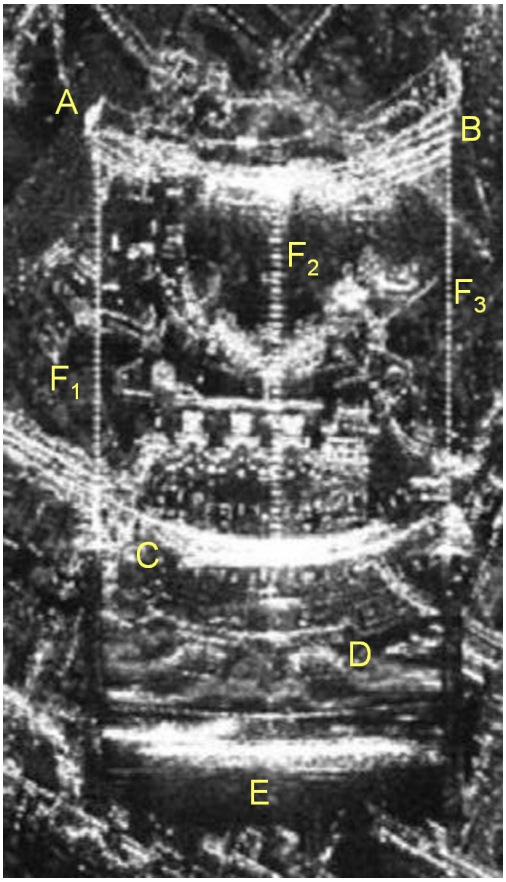

Fig. 9: TerraSAR-X image of hotel complex captured in spotlight mode; A - F: features to be compared with simulation; azimuth direction: left to right; range direction: top-down

A). This reflection effect is assumed to be caused by the roof of the hotel. Afterward, several lines are visible in the right part of the image showing strong contrast to the background (feature B). Moving on in range direction, a long transparent part ends at a bright arc which is assumed to contain double bounce contributions derived by the interaction between the hotel wall and the surrounding ground (feature C). Finally, after a region showing smeared features (feature D) and a broad line orientated in azimuth direction (feature E), a short shadow region starts. Furthermore, considering features orientated in range direction, three dashed lines are oriented in range direction (features F_1, F_2, F_3).

Google's 3D gallery provides a 3D model of the Wynn hotel in sketchup-format (©concept3D). Hence, in addition to visual interpretation of the image, the geometrical interpretation of these scattering effects can be supported by means of a simulated reflectivity map. To this end, the model is imported into our simulator where the geometrical model is completed by defining surface parameters, introducing a virtual sensor and constructing a flat plane beneath the building. The walls of the hotel are characterized by strong specular scattering combined with weak diffuse reflection and a high reflection coefficient. In the case of a detailed representation of roof structures in the 3D

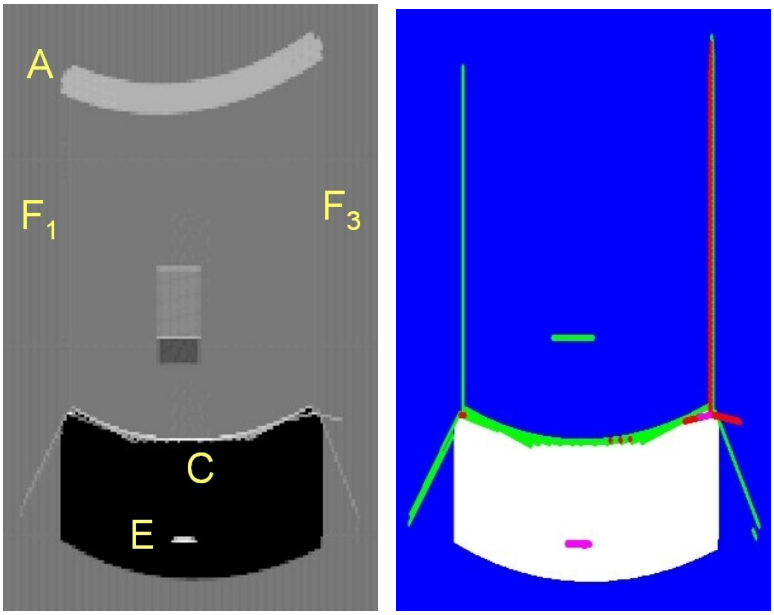

(a) Simulation (b) Distribution of reflection effects

Fig. 10: Result of Simulation (left), distribution of reflection effects (right): single bounce (blue), double bounce (green), triple bounce (red), fourfold bounce (magenta); azimuth direction: left to right; range direction: top-down

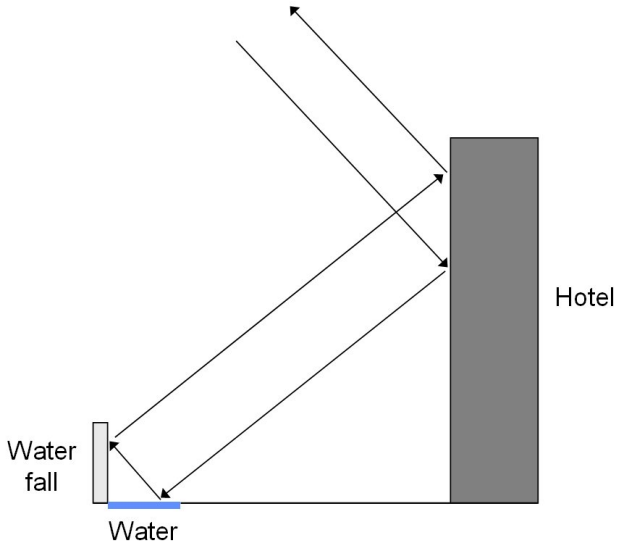

Fig. 11: Cross section through lake and hotel wall: fourfold bounce caused by interaction between walls and water surface

model, specular reflection characteristics would be more reasonable for roof parts since only the roof outline is actually visible in the SAR image. Here, strong diffuse scattering is assigned to the plane roof of the current 3D

model for emphasizing the extension the building and the shape of the roof. In order to be able to capture reflection effects caused by the waterfall, a simple concave wall model is shifted into the segment of the circle defined by the curved wall of the hotel. The concave appearance of the wall model has been designed by Constructive Solid Geometry by subtracting a sphere from a cube (see model on right part of Figure 8). Like for the walls of the hotel, the waterfall model is assumed to show strong specular reflection behavior.

The simulated reflectivity map including intensity values of bounce level 1 to 4 is shown on the left part of Figure 10. A map displaying the distribution of single or multiple scattering is shown in the right part of Figure 10, where colors blue, green, red and magenta correspond to single, double, triple and fourfold bounce, respectively.

At first, reflection effects showing up in both SAR image and reflectivity map are to be exemplified. Feature (A) is also included in the simulated image and is caused by the roof surface. Compared to the real SAR image, the area of the curved rectangle is not transparent in the artificial map since a high diffuse reflection component has been chosen for all parts of the roof. The assumption of feature (C) to be caused by double bounce between the hotel and the surrounding ground is confirmed by the simulator. Moreover, two additional lines showing up at both ends of feature (C) in the reflectivity map can be also identified in the real SAR image.

While the outline of the shadow zone is quite similar in both images, linear feature (E) is only hinted by the simulator and marked with bounce level 4. Figure 11 indicates how fourfold signals might be derived at the Wynn hotel complex, more specifically, by interaction of the signal with the hotel façade, the surface of the lake and the waterfall. As both the curvature of the building and curvature of the wall are orientated contrarily, spatial distances travelled by rays following the path ”sensor - building - water surface - water fall - building - sensor” within the POV Ray scene are almost similar. A complex multi-body 3D model of the area, which might be available in the future, could be used to further support the identification of objects causing fourfold bounce signals backscattered from the Wynn Hotel complex.

By using the distribution map (see Figure 10) two of three vertical dashed lines are classified as combination of double and triple bounce reflections at the wall of the hotel. The dashed line in the center of the hotel wall likely occurs due to double bounce effects caused by battens at almost all floors of the building. It is not possible to obtain this effect in the simulated image as all walls of the hotel have been modelled by means of flat surfaces. Contributions of surrounding buildings, vegetation or terrain are not visible, since they have not been designed in the model scene.

In case of the low quality Wynn Hotel model, information derived is not sufficient for interpreting all reflection effects in the SAR image, because most of them are caused by objects not included in the POV Ray model scene, e.g. features (B) or (D) do not appear in the simulation result. Nevertheless, artificial reflectivity maps can support the process of opinion making while observing and analyzing features in SAR images. Users of radar data should be aware of an increased number of deterministic reflection effects especially showing up in urban areas.

In the subsequent section, an example for the integration of 3D models of increased quality into the simulation process is given.

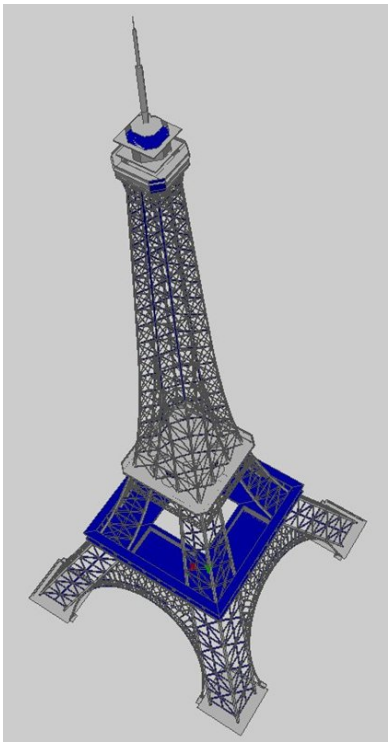

Fig. 12: 3D model of Eiffel Tower, Paris, France; ©SETE (www.tour-eiffel.fr)

C. Eiffel Tower

As the geometrical quality of the simulated reflectivity map mainly depends on the quality of the 3D model scene used for the simulation process, also models of high quality are to be illuminated by the virtual SAR sensor for analyzing further potentials and limits of our simulator.

A highly interesting example is, for instance, the Eiffel Tower (Paris) in order to compare images derived from the simulator to TerraSAR-X images. In this example, an amplitude mean map of 6 TerraSAR-X spotlight images (incidence angle: 34,6 degrees) has been generated to suppress speckle. The 3D model, which is shown in Figure 12, can be downloaded on www.tour-eiffel.fr for non-commercial purposes. It is composed by 9.488 facets and is offered in formats .obj (object format) and .dxf (AutoCAD format).

According to the SAR geometry given for the TerraSAR-X images, the tower was rotated and illuminated by the virtual sensor using the same signal incidence angle as for the real SAR images. The number of rays to be followed was chosen to 1.000 in azimuth times 4.000 in elevation yielding a sampling density of 0.2 m x 0.2 m in the model scene. Afterwards, the reflectivity map was created whose pixel spacing was adapted to the TerraSAR-X sampling, i.e. 0.43 m x 0.4 m in azimuth and ground range. The maximum number of bounces to be traced was fixed to 5 which was the maximum number for the Eiffel tower case as detected by the simulator (Figure 14a). With regard to processing time in case of the complex Eiffel tower model, both steps sampling and image creation took 5 minutes and 14 seconds on a standard computer (2 GHz Dual Core, 4 GB Ram). Concerning the radiometry, strong specular

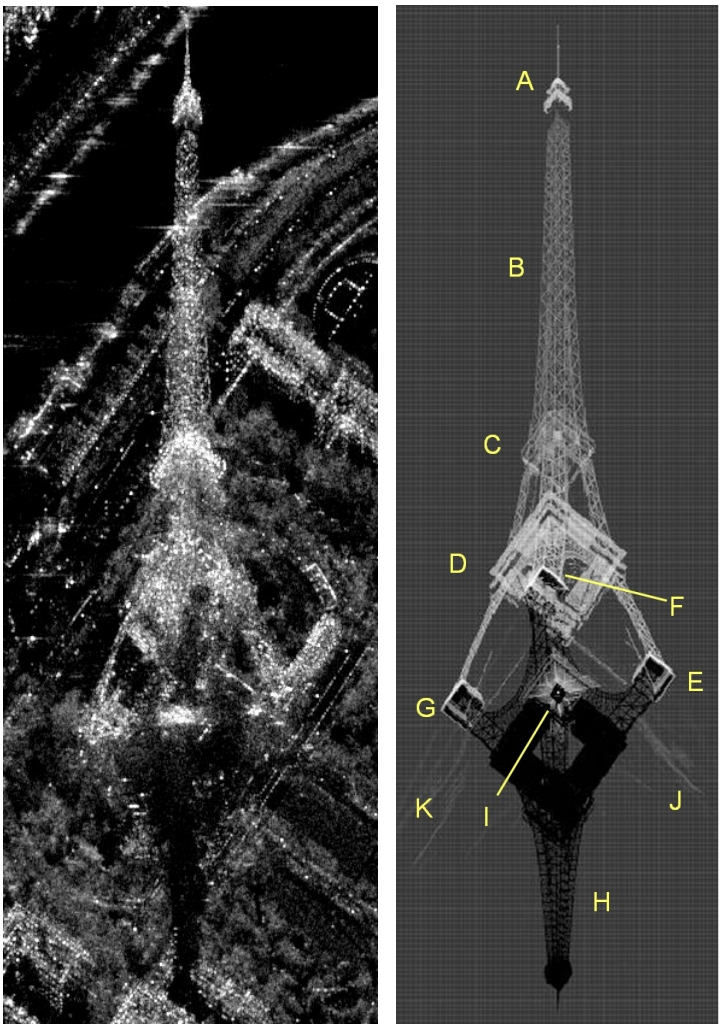

(a) Mean Map (b) Simulation

Fig. 13: Comparison: mean map obtained by averaging 6 spotlight TerraSAR-X images (left), reflectivity map (right); A: pinnacle; B: cross beam structures; C,D: plattforms; E,F,G: feet; H: shadow zone; I,J,K: double bounce contributions between tower and surrounding ground; azimuth direction: left to right; ground range direction: top-down

reflection behavior, a low amount of diffuse scattering and a high reflectivity factor were assigned to all surfaces of the tower. Since double bounce contributions caused by the interaction between tower and ground were to be considered, a flat plane was introduced into the model scene showing low diffuse reflection but strong reflectivity. Strong backscattering at cross beam structures was derived by means of strong specular reflection behavior for surfaces combined with mean diffuse reflection for considering local double bounce effects at the tower and signals backscattered by small features like nivets which have not been considered in the 3D model. Both the mean map

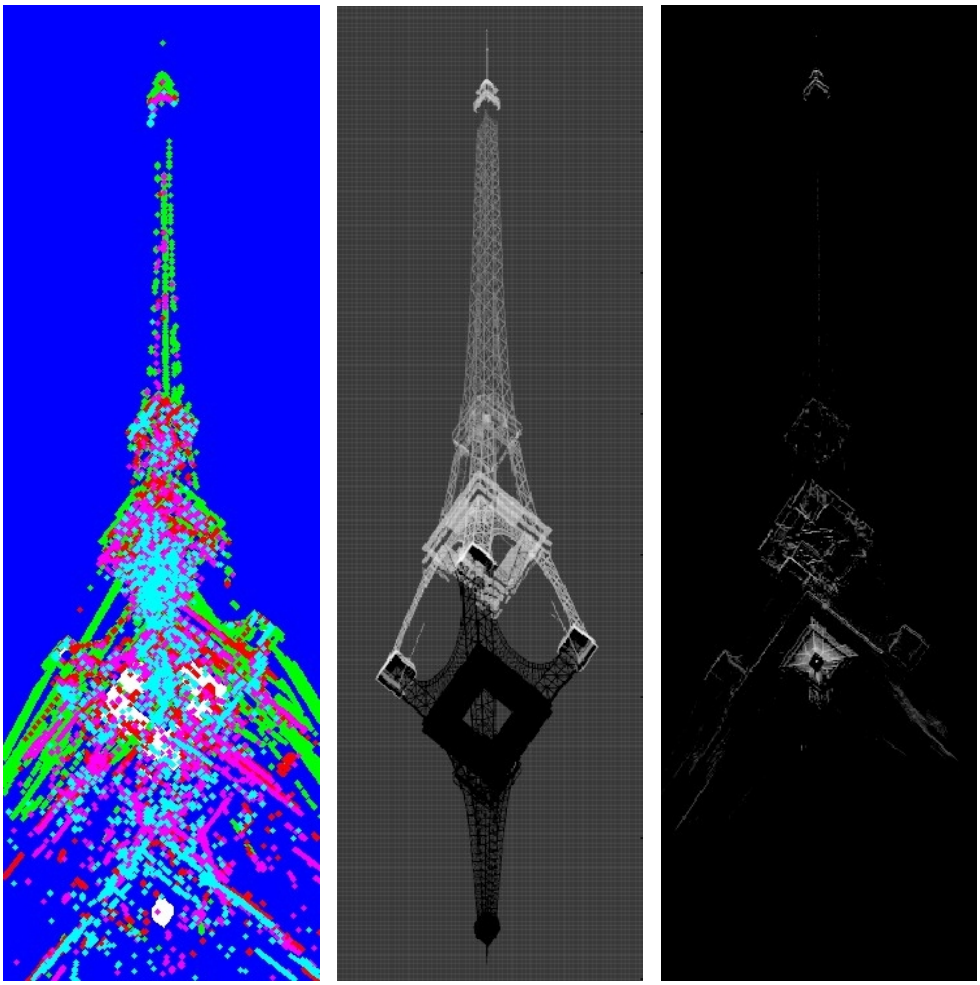

(a) Distribution (b) Single Bounce (c) Double Bounce

Fig. 14: Separation of bounce levels; left: distribution of reflection effects: single bounce (blue), double bounce (green), triple bounce (red), fourfold bounce (magenta), fivefold bounce (cyan); center and right: reflectivity maps of single and double bounce; azimuth direction: left to right; ground range direction: top-down

obtained by averaging 6 spotlight TerraSAR-X images and the simulation result are shown in Figure 13. The pixel spacing in the SAR mean map is 0.86 m x 0.8 m in azimuth and ground range due to a multi-looking factor of 2. Compared to the SAR image many features are also clearly visible in the reflectivity map derived by the 3D model scene of the tower. The shortest distance with respect to the SAR sensor is obtained for the pinnacle (A), followed by cross beam structures (B) in higher regions of the tower, two main plattforms (C, D), three visible feet of the tower (E, F, G) and the shadow zone (H). Obviously, during SAR simulation, a higher amount of signal power was able to penetrate the cross beam structures causing stronger single bounce backscattering in the background of the tower. By contrast, this region is almost completely shadowed in the SAR image where it appears

black. This might appear due to signal diffraction at tower crossbeams which is not considered in the simulation process. Compared to the real SAR case, objects in the neighborhood of the tower are neglected since the ground underneath the tower only has been modelled by means of a flat plane. Hence, overlay effects with other objects are not obtained in the simulation but clearly visible in the real SAR image, where features C to G are overlaid with diffuse backscattering contributions caused by vegetation in the park surrounding the tower. Further double bounce effects caused by the interaction between the tower and the surrounding ground show up at the bottom (I) and at both sides of the tower (J,K). While effect (I) is also apparent in the SAR image effects (J) and (K) likely dissappear because of buildings adjacent to the tower avoiding any backscattering to the sensor. Geometrical and radiometrical interpretation is supported by using the bounce level information in order to display different bounce levels in separated image layers (Figure 14b and 14c). While single bounce and double bounce cause strong intensities and hence clear structures in the reflectivity map, contributions of higher bounce levels are weakened by the decreasing weight factor of the ray followed through the modelled scene (see Section III-B). For this reason, threefold, fourfold and fivefold bounces are not displayed since their contributions show too little contrast to the background.

V. Conclusion & Outlook

In this paper a new approach for simulating SAR reflectivity maps has been presented. It extends the open-source ray tracing software POV Ray. The imaging SAR system is approximated by both a cylindrical light source and an orthographic camera. Reflection contributions are evaluated by following rays in reverse direction, i.e. starting at the center of each image pixel. Artificial images are derived by a processing chain containing three major steps: modeling of a virtual 3D object scene, sampling of the scene by rays and image creation in the azimuth-range plane. Simulation results created by means of 3D models of moderate and high quality have been shown for different purposes: 1.) for detection of deterministic double bounce effects, 2.) for fast classification of multiple bounce effects and 3.) for creating high resolution reflectivity maps.

Generally, the geometrical quality of resulting reflectivity maps is limited both by the level of detail of 3D models and the sampling density chosen by the operator, i.e. the area covered per pixel in the image plane of the orthographic camera. The radiometric quality is constrained by relying purely on specular and diffuse reflection models. Moreover, it has to be considered that discrete rays are sent through the model scene instead of continous waves.

Despite of these limits of the ray tracing approach, it has been shown that simulation of the geometrical distribution of scattering effects is helpful for supporting the interpretation of high resolution SAR images. Three-dimensional models of high complexity can be handled in our simulator to provide artificial reflectivity maps of high geometrical quality for comparison to real spaceborne SAR images. Most common model formats can be processed while computing time is low because of the optimized source code. Most important, different bounce levels can be assigned to separated layers for further geometrical analysis. Future work will concentrate on additional case studies at very detailed 3D models for detecting backscattered signals caused by small building features. Strong

reflection zones visible in the reflectivity map are to be mapped back into the 3D model for identifying areas causing strong double or multiple bounce effects. Future developments will focus on evaluating potentials for tomographic analysis of reflection effects in 3D since, so far, information along the elevation direction has not been included in the backscattering analysis.

REFERENCES

[1] S. Ochs and W. Pitz, "The TerraSAR-X and TanDEM-X satellites," in *Proceedings of 3rd International Conference on Recent Advances in Space Technologies*, June 2007, pp. 294–298.

[2] P. Lombardo, "A multichannel spaceborne radar for the COSMO-Skymed satellite constellation," *Proceedings of IEEE Aerospace Conference*, vol. 1, pp. 111–119, March 2004.

[3] U. Stilla, "High resolution radar imaging of urban areas," in *Photogrammetric Week*, D. Fritsch, Ed., Stuttgart, 2007, pp. 149–158.

[4] R. Bamler and M. Eineder, "The pyramids of gizeh seen by TerraSAR-X - a prime example for unexpected scattering mechanisms in SAR," *Geoscience and Remote Sensing Letters, IEEE*, vol. 5, no. 3, pp. 468–470, July 2008.

[5] S. Gernhardt, S. Hinz, N. Adam, and R. Bamler, "Enhancements for persistent scatterer interferometry with high resolution SAR," in *Proceedings of FRINGE 2007*, Frascati, 2007, p. on CD.

[6] S. Auer, S. Gernhardt, S. Hinz, N. Adam, and R. Bamler, "Simulation of radar reflection at man-made objects and its benefits for persistent scatterer interferometry," in *Proceedings of the 7th European Conference on Synthetic Aperture Radar (EUSAR 2008)*, Friedrichshafen, 2008.

[7] N. Adam, M. Eineder, N. Yague-Martinez, and R. Bamler, "High resolution interferometric stacking with TerraSAR-X," in *IEEE International Geoscience and Remote Sensing Symposium, 2008. IGARSS 2008.*, 2008.

[8] G. Franceschetti, M. Migliaccio, D. Riccio, and G. Schirinzi, "SARAS: a synthetic aperture radar (SAR) raw signal simulator," *IEEE Transactions on Geoscience and Remote Sensing*, vol. 30, no. 1, pp. 110–123, Jan. 1992.

[9] G. Franceschetti, A. Iodice, and D. Riccio, "A canonical problem in electromagnetic backscattering from buildings," *IEEE Transactions on Geoscience and Remote Sensing*, vol. 40, no. 8, pp. 1787–1801, Aug 2002.

[10] G. Franceschetti, A. Iodice, D. Riccio, and G. Ruello, "SAR raw signal simulation for urban structures," *IEEE Transactions on Geoscience and Remote Sensing*, vol. 41, no. 9, pp. 1986–1995, Sept. 2003.

[11] T. Balz, "Real-time SAR simulation of complex scenes using programmable graphics processing units," in *Proceedings of the ISPRS TCVII Mid-term Symposium*, Enschede, 2006.

[12] G. Margarit, J. J. Mallorqui, J. M. Rius, and J. Sanz-Marcos, "On the usage of GRECOSAR, an orbital polarimetric SAR simulator of complex targets, to vessel classification studies," *IEEE Transactions on Geoscience and Remote Sensing*, vol. 44, no. 12, pp. 3517–3526, Dec. 2006.

[13] G. Margarit, J. J. Mallorqui, and C. Lopez-Martinez, "GRECOSAR, a SAR simulator for complex targets: Application to urban environments." in *IEEE International Geoscience and Remote Sensing Symposium IGARSS 2007*, J. J. Mallorqui, Ed., Barcelona, 2007, pp. 4160–4163.

[14] J. Rius, M. Ferrando, and L. Jofre, "GRECO: graphical electromagnetic computing for RCS prediction in real time," *Antennas and Propagation Magazine, IEEE*, vol. 35, no. 2, pp. 7–17, April 1993.

[15] D. Brunner, G. Lemoine, and L. Bruzzone, "Height estimation of man made structures using hybrid VHR optical and SAR imagery," in *Proceedings of Remote Sensing - New Challenges of High Resolution, EARSeL Joint Workshop*, Bochum, 2008.

[16] H. Hammer, T. Balz, E. Cadario, U. Soergel, U. Thoennessen, and U. Stilla, "Comparison of SAR simulation concepts for the analysis of high resolution SAR data," in *Proceedings of the 7th European Conference on Synthetic Aperture Radar (EUSAR 2008)*, Friedrichshafen, 2008.

[17] S. Gernhardt and S. Hinz, "Advanced displacement estimation for PSI using high resolution SAR data," *IEEE International Geoscience and Remote Sensing Symposium, 2008. IGARSS 2008.*, vol. 3, pp. III –1276–III –1279, July 2008.

[18] A. Ferretti, C. Prati, and F. Rocca, "Permanent scatterers in SAR interferometry," *IEEE Transactions on Geoscience and Remote Sensing*, vol. 39, no. 1, pp. 8–20, Jan 2001.

[19] B. Kampes, *Radar Interferometry - Persistent Scatterer Technique*, F. van der Meer, Ed. Dordrecht, The Netherlands: Springer, 2006.

[20] R. Guida, A. Iodice, D. Riccio, and U. Stilla, "Model-based interpretation of high-resolution SAR images of buildings," *Selected Topics in Applied Earth Observations and Remote Sensing, IEEE Journal of*, vol. 1, no. 2, pp. 107–119, June 2008.

[21] www.povray.org [last access: 28.07.2009], Persistence of Vision Raytracer Propriety Limited.

[22] R. Wolfe, *3D Graphics: A Visual Approach*, R. Wolfe, Ed. Oxford University Press, Sept. 1999.

[23] T. Lama, *3D-Welten*, T. Lama, Ed. Muenchen: Hanser, 2004.

[24] C. M. Hoffmann, *Geometric & Solid Modeling*. Morgan Kaufmann Publishers, San Mateo, California, 1989. [Online]. Available: http://www.cs.purdue.edu/homes/cmh/distribution/books/geo.html

[25] A. S. Glassner, *An Introduction to Ray Tracing*, 9th ed., A. S. Glassner, Ed. San Francisco: Morgan Kaufmann, 2002.

[26] B. Phong, "Illumination for computer generated pictures," *Communications of the ACM 18*, vol. 18, no. 6, pp. 311–317, 1975.

[27] T. Whitted, "An improved illumination model for shaded display," *Commun. ACM*, vol. 23, no. 6, pp. 343–349, 1980.

[28] L. Tsang and J. Kong, *Scattering of Electromagnetic Waves: Advanced Topics*, L. Tsang and J. Kong, Eds. John Wiley & Sons, Inc., New York, 2001.

[29] J. Groot and M. Otten, "SAR imaging of corner reflectors larger than the spatial resolution," *IEEE Transactions on Geoscience and Remote Sensing*, vol. 32, no. 3, pp. 721–724, May 1994.

[30] A. Reigber and A. Moreira, "First demonstration of airborne SAR tomography using multibaseline L-band data," *IEEE Transactions on Geoscience and Remote Sensing*, vol. 38, no. 5, pp. 2142–2152, Sep 2000.

[31] G. Fornaro, F. Serafino, and F. Soldovieri, "Three-dimensional focusing with multipass SAR data," *IEEE Transactions on Geoscience and Remote Sensing*, vol. 41, no. 3, pp. 507–517, March 2003.

[32] X. Zhu, N. Adam, and R. Bamler, "First demonstration of space-borne high resolution SAR tomography in urban environment using TerraSAR-X data," in *Proceedings of CEOS SAR Workshop on Calibration and Validation*, 2008.

[33] A. Thiele, E. Cadario, K. Schulz, U. Thonnessen, and U. Soergel, "Building recognition from multi-aspect high-resolution InSAR data in urban areas," *IEEE Transactions on Geoscience and Remote Sensing*, vol. 45, no. 11, pp. 3583–3593, Nov. 2007.

[34] U. Soergel, U. Thoennessen, A. Brenner, and U. Stilla, "High-resolution SAR data: new opportunities and challenges for the analysis of urban areas," *IEE Proceedings - Radar, Sonar and Navigation*, vol. 153, no. 3, pp. 294–300, June 2006.

Stefan Auer was born in Bad Reichenhall, Germany, on April 17, 1980. In December 2005 he graduated from the TUM (Technische Universität München) with a Dipl.-Ing.(Univ.) degree in Geodesy and Geoinformation. Since December 2006 he is full-time scientific colaborator at Remote Sensing Technology of TUM and pursues his PhD on the simulation of radar reflection effects by means of 3D models of high quality. His work is part of the project team 'Dynamic Earth' which was established in the International Graduate School of Science and Engineering (IGSSE) at TUM as a result of the german excellence initiative in 2007. In February/March 2008 and 2009, he spent 9 weeks at the Department of Electronic and Telecommunication Engineering (DIET) at the University of Naples "Federico II", where he busied himself with the theory of electromagnetic field propagation at man-made objects.

His main interest is in supporting the interpretation of high resolution SAR images by generating reflectivity maps and separating deterministic reflection effects of different bounce levels.

Stefan Hinz (born 1972) graduated from the Technische Universität München (TUM) with a Dipl.-Ing. degree in Geodesy and Geoinformation in 1998. He received the Dr.-Ing. degree with "summa cum laude" for his PhD work on Automatic Extraction of Urban Road Networks from Aerial Images in 2003 and the venia legendi ("Habilitation") for his work on Moving Object Detection and Monitoring in Remote Sensing Data in 2008, both from TUM. Since December 2008, Stefan Hinz is full professor for Remote Sensing and Computer Vision and head of the Institute for Photogrammetry and Remote Sensing at Universität Karlsruhe.

In 1999, he was guest researcher at the Institute of Robotics and Intelligent Systems (IRIS) of the University of Southern California at Los Angeles. The research conducted at IRIS was funded by the German Academic Exchange Service by a grant.

His research interests include various aspects of computer vision and image understanding, especially theory and methods for the automatic extraction, characterization and monitoring of natural and infrastructural objects in optical, infrared, Lidar and Radar remote sensing data.

Richard Bamler (M'95–SM'00–F'05) received his diploma degree in electrical engineering, his doctor of engineering degree, and his "habilitation" in the field of signal and systems theory in 1980, 1986, and 1988, respectively, from the Technische Universität München (Germany).

He worked at that university during 1981 and 1989 on optical signal processing, holography, wave propagation, and tomography. He joined the German Aerospace Center (DLR), Oberpfaffenhofen, in 1989, where he is currently the Director of the Remote Sensing Technology Institute. Since then he and his team have been working on SAR signal processing algorithms (ERS, SIR-C/X-SAR, Radarsat, SRTM, ASAR, TerraSAR-X, TanDEM-X), SAR calibration and product validation, SAR interferometry, phase unwrapping, estimation theory and model based inversion methods for atmospheric sounding (GOME, SCIAMACHY, MIPAS, GOME-2) and oceanography.

In early 1994 Prof. Bamler was a visiting scientist at Jet Propulsion Laboratory (JPL) in preparation of the SIC-C/X-SAR missions, and in 1996 he was guest professor at the University of Innsbruck. Since 2003 he holds a full professorship in remote sensing technology at the Technische Universität München.

His current research interests are in algorithms for optimum information extraction from remote sensing data with emphasis on SAR, SAR interferometry, persistent scatterer interferometry, SAR tomography, and GMTI for traffic monitoring. He and his team have recently developed and are currently developing the operational processor systems for the German missions TerraSAR-X, TanDEM-X, EnMAP, and MetOp/GOME-2.

Richard Bamler is the author of more than 150 scientific publications, among them about 35 journal papers, a book on multidimensional linear systems theory, and several patents on SAR signal processing.